

Spatially resolved stellar population parameters in the BCGs of two fossil groups

Robert N. Proctor^{1,2}, Claudia Mendes de Oliveira¹, Paul Eigenthaler³

¹ *Universidade de São Paulo, IAG, Rua do Matão, 1226, São Paulo, 05508-090, Brasil*

² *Observatório Nacional, Rua Gal. José Cristino, 20921-400, Rio de Janeiro, Brazil*

³ *Instituto de Astronomía y Astrofísica, Pontificia Universidad Católica de Chile, Av. Vicuña Mackenna 4860, Santiago, Chile*
email: rnp059@gmail.com

15 January 2014

ABSTRACT

We report the results of Gemini/GMOS long-slit spectroscopic observations along the major and minor axes of the central galaxies in two fossil groups, SDSS J073422.21+265133.9 and SDSS J075828.11+374711.8 (the NGC 2484 group). Spatially resolved kinematics and stellar population parameters (ages, metallicities and α -element abundance ratios) derived using ~ 20 Lick indices are presented. Despite remarkable similarities in their morphologies, photometric properties (luminosity and colour) and kinematics, the two galaxies exhibit significantly different stellar population parameters.

SDSS J073422.21+265133.9 exhibits a strong metallicity gradient ($\Delta [Z/H]/\Delta R \sim -0.4$) all the way into the centre of the galaxy. It also exhibits an age profile that suggest a relatively recent, centrally concentrated burst of star formation superimposed on an older, more spatially extended population. NGC 2484, a well known X-ray AGN, exhibits a flat core-like structure in its metallicity gradient, but no detectable age gradient. The α -element abundance ratio ($[E/Fe]$) profiles of the two galaxies are also significantly different. SDSS J073422.21+265133.9 exhibits a slightly positive gradient ($\Delta [E/H]/\Delta R \sim 0.1$), perhaps again suggesting a more recent central burst of star formation, while NGC 2484 shows a negative gradient ($\Delta [E/H]/\Delta R \sim -0.1$), indicating that star formation may have happened "inside out".

Our analysis of these two galaxies of similar mass, morphology and kinematics therefore suggests two different mechanisms to have been in action during their formation. Consequently, we conclude that the central galaxies of fossil groups can not be considered a homogeneous group with regard to their formation processes or star formation histories.

Key words: galaxies: groups: general – galaxies: elliptical and lenticular, cD – galaxies: stellar content – galaxies: kinematics and dynamics

1 INTRODUCTION

Fossil galaxy groups are defined as X-ray luminous ($L_{X, \text{bol}} > 0.5 \times 10^{42} h_{50}^{-2} \text{ erg s}^{-1}$) galaxy aggregates with a greater than 2 magnitude gap between the brightest and second brightest galaxies within half the virial radius (Jones et al. 2003). The commonly stated paradigm for the formation of these systems is that the large magnitude gap is generated by dynamical friction acting on the massive L^* galaxies near the centre of the group, which causes them to spiral inwards and merge with the central galaxy. For the magnitude gap to be sustained, this scenario requires the group undergoes no significant recent mergers or infall events. According to this paradigm, fossil groups therefore represent highly evolved, but otherwise undisturbed, exam-

ples of galaxy groups that formed early in the history of the universe. Hence the study of fossil groups has become of great interest, as this scenario suggests that they represent the undisturbed end-product of galaxy group evolution. Contrary to this hierarchical merging scenario it was also suggested that fossil groups could simply be *failed groups* that formed with a top-heavy luminosity function absent of L^* galaxies (Mulchaey & Zabludoff 1999). As such they represent an important benchmark against which other systems can be compared.

Although fossil groups as whole systems are believed to have collapsed early and have assembled most of their virial masses at higher redshifts, in comparison with non-fossil groups (D’Onghia et al. 2005; Dariush et al. 2007),

first-ranked galaxies in fossil groups may have merged *later* than non-fossil bright central galaxies (Díaz-Giménez et al. 2008). The question to which this work is addressed is then: does the formation process of fossil groups create significant differences in the stellar population gradients of their first-ranked galaxies when compared to non-fossil bright cluster galaxies (hereafter BCGs)?

There are relatively few studies on the stellar population gradients of BCGs, and for fossil groups, only one study has been carried-out so far, concluding that first-ranked galaxies in fossil groups show comparatively flat metallicity gradients indicative of a major merger origin (Eigenthaler & Zeilinger 2013). Loubser & Sánchez-Blázquez (2012) presented a systematic study of the relations between the stellar population gradients of 24 BCGs in non-fossil clusters and properties of the cluster where they reside (richness, mass, etc). This study may serve as a benchmark against which results on the properties of first-ranked galaxies of fossil groups can be compared. Other smaller samples which focused on the detailed study of stellar populations of BCGs are Brough et al. (2007); Spolaor et al. (2009); Gorgas et al. (1990); Fisher et al. (1995); Sánchez-Blázquez et al. (2006); Mehlert et al. (2003); Carter et al. (1999); Davidge & Grindler (1995). Studies of BCGs in non-fossil groups have shown that these galaxies possess central stellar populations that are generally old, of super solar metallicity and moderately α -element enhanced, i.e. they exhibit similar ages and metallicities as non-BCGs of the same mass. However, some studies hint towards higher $[\text{E}/\text{Fe}]$ values in BCGs (von der Linden et al. 2007; Loubser et al. 2009). BCGs exhibit fairly strong negative metallicity gradients, and shallow age gradients, both positive and negative. Where available α -element abundance ratios are shown to be relatively shallow (Loubser & Sánchez-Blázquez 2012). However, it is not simple to infer a consistent formation history for BCGs that can at the same time explain the gradients in the three parameters, age, metallicity, and abundances. In any case, what is evident is that the dispersions in the stellar population parameters are high, indicating a number of possible formation scenarios for BCGs that depend on the details of the merging history for each galaxy.

Given our small sample, a full statistical comparison of fossil to non-fossil BCGs is not possible in this paper, but must wait until a larger sample of first-ranked fossil group galaxies have been studied at the same level of detail. In this work we therefore simply continue the accumulation of stellar population parameters age, $[\text{Fe}/\text{H}]$, $[\text{E}/\text{Fe}]$ (a proxy for $[\alpha/\text{Fe}]$ (Proctor & Sansom 2002)), and $[\text{Z}/\text{H}]$ for BCGs in fossil groups.

The paper is organised as follows. In Section 2 the sample selection, observations and data reduction are described. Section 3 presents galaxy kinematics and stellar population parameters. Section 4 discusses the obtained results while Sect. 5 shows our conclusions.

2 SAMPLE SELECTION, OBSERVATIONS AND DATA REDUCTION

We report on Gemini GMOS spectroscopic data for the BCGs of the two fossil groups SDSS J073422.21+265144.9 and SDSS J075828.10+374711.8 (hereafter SDSS0734 and SDSS0758). The sample was selected from the list of fossil groups in Díaz-Giménez et al. (2008), originally identified in the Sloan Digital Sky Survey (SDSS) DR6 (Adelman-McCarthy et al. 2008). Díaz-Giménez et al. (2008) used a Friends-of-Friends analysis to find groups within the SDSS with an over-density contrast of 200, more than 10 spectroscopically confirmed members, masses greater than $5 \times 10^{13} h^1 \text{ M}_\odot$ and redshifts lower than 0.1. Using these criteria, Díaz-Giménez et al. (2008) identified five groups with Δm_{12} values larger than 2.0. We had originally intended to observe all five bona-fide fossil groups from Díaz-Giménez et al. (2008), however, given the time allocation constraints, we obtained data for only two of them (galaxies II and IV in Díaz-Giménez et al. 2008). The two galaxies possess nearly identical photometric properties and reside in groups with very similar properties. Their g band magnitudes, $g - r$ colours, sizes, minor/major axis ratios (b/a), and redshifts are given in Table 1. The Δm_{12} values, velocity dispersions, number of spectroscopically confirmed members within the virial radius and richness of the groups in which these BCGs reside are also given in Table 1. Magnitudes, colours and redshifts were taken from the SDSS DR9. The absolute g band magnitude was taken from the SDSS DR9 photoz table. For effective radii, we considered the isophotal radius at $\mu_K = 20 \text{ mag arcsec}^{-2}$ from the 2MASS extended objects catalogue (Skrutskie et al. 2006) to be a good estimate (see also Proctor et al. 2008). Based on the photometric similarities of both galaxies and the groups in which they reside, the selected targets are ideal for studying the uniformity of the formation scenario for fossil galaxy groups. Hence we carried out spectroscopic observations along the major and minor axes of these two fossil BCGs to study their spatially resolved stellar population parameters.

The observations were performed using GMOS on Gemini North on December 24 in 2011 (GN-2011B-Q-107) in long-slit mode. Observations were carried out using the B600+G5307 grating and a long-slit of 1 arcsec slit-width, yielding a dispersion of $0.92 \text{ Å pixel}^{-1}$. We measured a spectral resolution of 4.7 Å over a wavelength range of 3500 to 6300 Å from the FWHM of multiple arc calibration lines. Three exposures of 1800 s were performed along each of the major and minor axes of both galaxies. Exposures were dithered in the spectral direction in order to provide coverage across the GMOS chip gaps¹. Arc and flat-field observations were interleaved between the target exposures. The bias frames provided by the observatory were taken from a preceding run on December 12 in 2011. The seeing was $\geq 1.2 \text{ arcsec}$.

The data reduction was carried out using the IRAF Gemini GMOS package and STARLINK software. Early in the data reduction process, it became apparent that the data suffered from significant contamination by scattered light, which had serious repercussions for flat-fielding and sky-subtraction. In order to minimise scattered light effects, the reduction procedure carried out differed slightly from

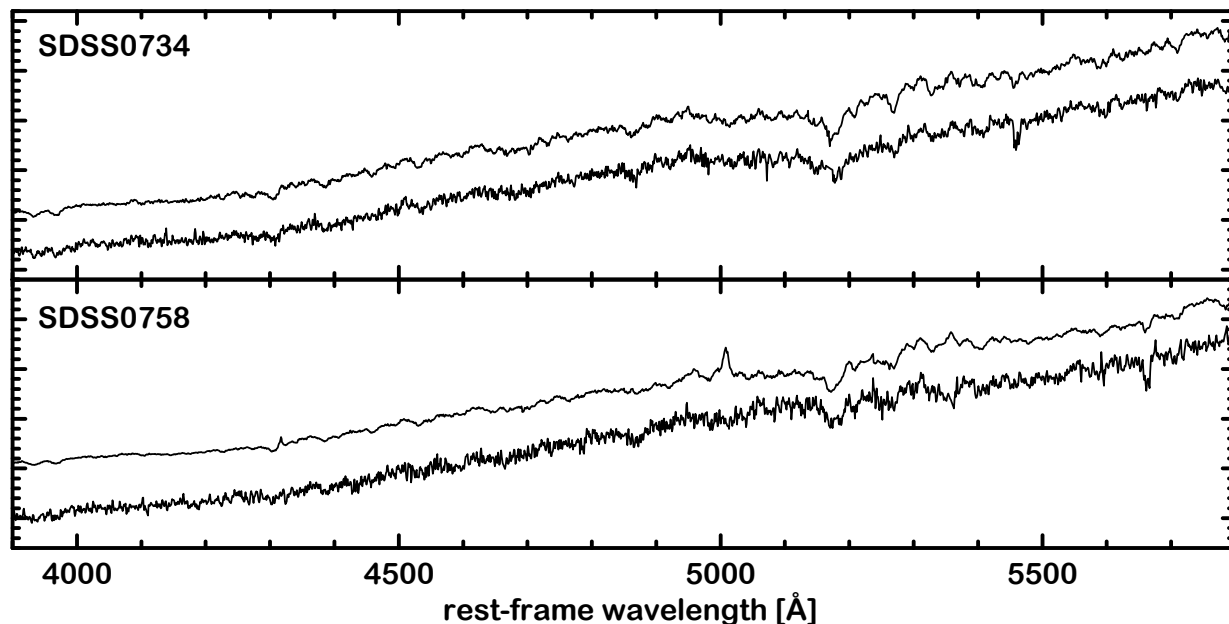


Figure 1. De-redshifted spectra along the major axis of the observed BCGs of the two fossil groups. The central bin and one in the outskirts around $\log(r/r_{\text{eff}}) \sim -0.3$ are shown. Sky-line residuals have been removed for better visualisation. The spectra have been normalised to the flux at $\lambda 5000\text{\AA}$. SDSS0758 shows prominent [OIII] $\lambda\lambda 4959, 5007\text{\AA}$ emission in the center and is a well-known X-ray AGN (Sun 2009).

Table 1. Overall properties of the observed fossil BCGs and the groups in which they reside.

BCGs	SDSS0734	SDSS0758
α_{J2000}	07 ^h 34 ^m 22 ^s .2	07 ^h 58 ^m 28 ^s .1
δ_{J2000}	+26° 51′ 44″.9	+37° 47′ 11″.8
g [mag]	15.35	13.87
M_g [mag]	−22.67	−22.58
$g - r$ [mag]	1.00	0.89
r_{eff} [arcsec]	15.2	30.2
r_{eff} [kpc]	24.1	25.7
b/a	0.80	0.78
z	0.0796	0.0408
Groups	SDSS0734	SDSS0758
Δm_{12} [mag]	2.01	2.64
σ [km s ^{−1}]	551	563
Members	16	38
Richness	5	4

Notes: Magnitudes, colours and redshifts were taken from the SDSS DR9, while coordinates, minor/major axis ratios, and effective radii were taken from NED. Members is the number of galaxies within the virial radius with SDSS spectroscopy. Group richness is defined as the number of spectroscopically confirmed members brighter than $0.4L^*$.

the usual sequence. First, both target and flat-field frames were bias subtracted, cleaned of cosmic rays and bad pixels, and subsequently wavelength calibrated using Cu-Ar comparison-lamp exposures. Next we used the only regions in our observations in which the scattered light could be measured directly, i.e. the *bridges* in the long-slit¹, to estimate scattered light levels, again in both target and flat-

field frames. We found that some 20% of the light reaching the detector was in the form of scattered light. Estimates of the scattered light contamination were made by interpolating between the two bridges, along the spatial direction. These levels were then subtracted from each exposure. Flat-fielding of the decontaminated target frames was then carried out using the corrected flat-field frames. The resultant light profiles along the spatial direction were found to be much flatter at large radii, i.e. more consistent with the constant sky level one would expect at such radii. Sky subtraction was then performed in the usual manner, by fitting a linear function to background windows along the spatial direction on each side of the galaxy spectrum outside the effective radii. The data were then binned along each axis so that the outer bins still yielded a reasonable S/N. In the center, typically 2 pixels were binned while in the outskirts, around r_{eff} , about 50 pixel rows were added. We measure a typical S/N of ~ 70 in the center and ~ 15 in the outskirts. Figure 1 shows spectra along the major axes for both galaxies. The central bin and one in the outskirts around $\log(r/r_{\text{eff}}) \sim -0.3$ are presented.

3 KINEMATICS AND STELLAR POPULATION PARAMETERS

The recession velocities and velocity dispersions of each bin along the major and minor axes were measured using the IRAF fxcor routine. Bruzual & Charlot (2003) SSP models that had been broadened to the Gemini resolution of 4.7\AA were used as templates for this procedure. The SSP model showing the highest cross-correlation peak was selected for the final measures. However, variation in the values derived using different templates was found to be less than the er-

¹ see the definition of GMOS chip gaps and bridges on the Gemini homepage <http://www.gemini.edu/node/10663>

rors quoted in our results. The resulting values are shown in Fig. 2. Radial velocities are shown with respect to the systemic velocities. We find no evidence for rotation along either axis of either galaxy. The velocity dispersion profiles are both shallow. Indeed, there is no evidence for any reduction in velocity dispersion with radius in SDSS0758. It is therefore clear that both galaxies reside in substantial dark matter halos. The systemic velocities of both galaxies and the measured central values of the velocity dispersion are listed in Table 2. Radial velocities and velocity dispersions at each radial bin are given in Appendix A.

3.1 Measurement of stellar population parameters

To derive stellar population parameters, Lick/IDS line-strength indices as defined in Worthey et al. (1994) and Worthey & Ottaviani (1997) have been measured. The data were corrected for internal velocity dispersion as described in Proctor & Sansom (2002). In the absence of Lick standard star observations, full calibration to the Lick system could not be performed. However, as noted in many previous studies (e.g. Proctor & Sansom 2002), the only indices that significantly depend on such a calibration are Mg_1 and Mg_2 . These indices were therefore omitted from all further analysis. NaD was also excluded because of its contamination by interstellar absorption. The observed wavelength range did not cover the redshifted TiO indices. As a result a total of 22 Lick indices from H δ to Fe5782 were measured with 20 of these used in our analysis. The measurement of stellar population parameters age, $[Z/H]$ and $[E/Fe]$ was then carried out using the multi-index χ^2 -fitting technique detailed in Proctor & Sansom (2002). $[Fe/H]$ was then derived from $[Z/H]$ and $[E/Fe]$ using $[Fe/H] = [Z/H] - 0.94[E/Fe]$. The 20 indices were fit, first subject to three-sigma clipping. This removed indices contaminated by effects such as sky-line residuals and chip gap residuals as well as highlighting positions in the galaxies affected by emission lines (in this case the central two pixels of SDSS0758 only). The stability of the fits with respect to the exclusion of the remaining indices was then tested to ensure that no individual index was creating tension in the fit. In most cases the indices causing such tensions were found to be remaining sky-line residuals, or other clear distortions in the spectrum. Those indices were also excluded from the final fits. The resultant fits generally included between 17 and 20 indices. The derived stellar population parameters are shown in Fig. 3.

3.2 Comparison with full-spectrum fitting

To verify the stability of our measurements, we also compared our results from the multi-index χ^2 -fitting technique with a full-spectrum fitting technique. Therefore, the open-source package ULYSS (Koleva et al. 2009) was used to fit SSP models directly to the observed galaxy spectra. We utilized Pegase HR models resolved in $[\alpha/Fe]$ (Prugniel & Koleva 2012) based on the Elodie 3.2 library of stellar spectra (Wu et al. 2011)². The library involves an interpolator to provide a stellar spectrum at any point in the parameter space (T_{eff} , $\log g$, $[Fe/H]$, and $[\alpha/Fe]$). All

Pegase HR models are computed assuming a Salpeter IMF and Padova 1994 evolutionary tracks providing synthetic SSPs with ages between 1–20000 Myr, metallicities between -2.3 and 0.69 dex, and $[\alpha/Fe]$ enhancement between 0 and 0.4. A multiplicative polynomial is used to adjust the overall spectral shape to the SSP model. To achieve reasonable values an order of 40 was chosen. The ULYSS parameter `\CLEAN` was considered in the fitting procedure to exclude possible outliers in the galaxy spectrum, resulting from any remaining night sky emission. 200 Monte-Carlo simulations were computed for every spectral bin, repeating a fit successively with random Gaussian noise. The dimension of the added noise was based on a user-defined signal-to-noise ratio provided for each spectral bin. The S/N ratios were measured with IRAF `splot` at a rest-frame wavelength of ~ 5140 Å. The resulting point distributions were then used to calculate average SSP ages, $[Fe/H]$ (see also Eigenthaler & Zeilinger 2013) and $[\alpha/Fe]$ values. $[Z/H]$ was then also calculated from these data using $[Z/H] = [Fe/H] + 0.94[E/Fe]$. Outliers clearly detached from the main point distributions have been excluded for these measurements. Error bars were estimated as the standard deviation of the point distributions. For the comparison, we analysed the major axis spectra of both galaxies with ULYSS, and averaged the stellar population parameters from both galaxy sides.

Besides stellar population parameters, ULYSS also allows us to measure the kinematic properties of our galaxies since the package measures the shift in wavelength and broadening of each SSP model to match the observed galaxy spectrum. ULYSS determines the broadening relative to the SSP model dispersion σ_{model} , amounting to 13 km s^{-1} for the Pegase HR models. Taking into account instrumental dispersion, velocity dispersions are computed via the relation: $\sigma_{\text{phys}}^2 = \sigma_{\text{ulyss}}^2 + \sigma_{\text{model}}^2 - \sigma_{\text{instr}}^2$.

We also investigated the use of composite stellar populations within ULYSS by attempting to fit the *relatively* high S/N central bins of each galaxy with a combination of two independent SSPs. However, even in these central bins the S/N was not sufficient to permit the convergence of the fits to a stable solution given the large number of free parameters in such a fit. Therefore we report here only fits utilising single SSP models.

Figure 4 shows the comparison of our results from the multi-index χ^2 -fitting technique with the corresponding values derived from ULYSS full-spectrum fitting. We confirm the kinematic properties of both galaxies. However, we note that our ULYSS results show systematically larger values for velocity dispersion with an average offset of $\sim 30 \text{ km s}^{-1}$ compared to the values derived from the IRAF `fxcor` routine. The cause of this slight discrepancy remains unidentified. However, the offset (which is only slightly larger than the velocity dispersion errors) was found to have no significant effect on the stellar population parameters derived.

Qualitatively, both the kinematic and stellar population trends show fair agreement. However, there are some noticeably quantitative differences in the results of the stellar population analyses. Most noticeably, the $[E/Fe]$, although showing similar gradients, are systematically lower in the ULYSS full spectral fitting results. There are also some slight systematic differences in the derived $[Fe/H]$ values. For SDSS0734 we confirm the negative $[Fe/H]$ gradient but find a shallower slope, while for SDSS0758, we confirm the

² <http://ulyss.univ-lyon1.fr/optional.html>

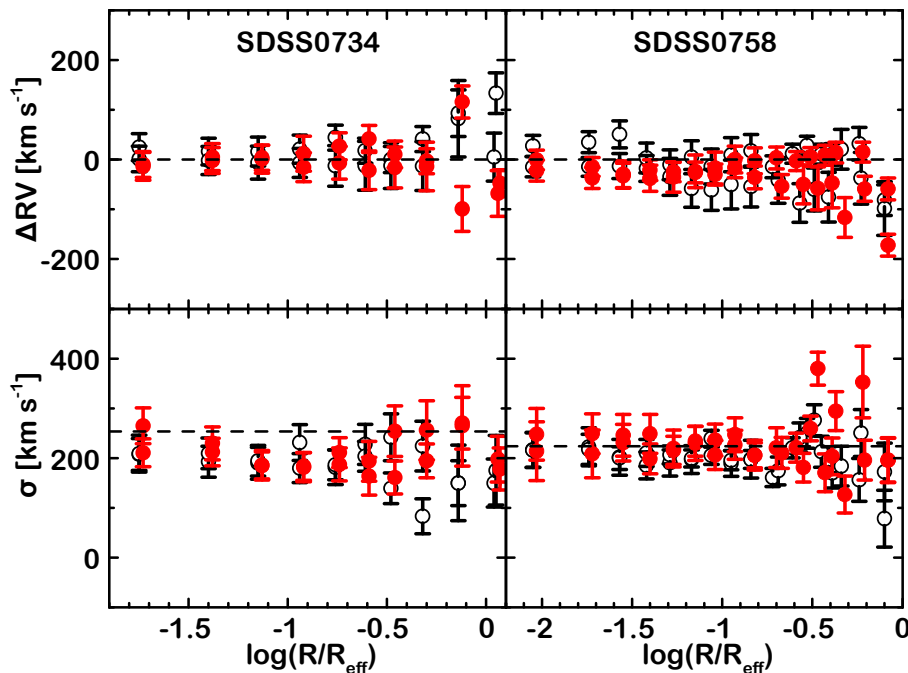


Figure 2. Kinematics of the observed BCGs of the two fossil groups. Radial velocity and velocity dispersion profiles are shown. Red points are measured along the major axis while open ones present the minor axis. The horizontal lines show the systemic velocities and central velocity dispersions. There is no evidence for rotation along either axis of either galaxy. The velocity dispersion profiles are both shallow.

flat inner metallicity gradient, but find a flat gradient also at larger galactic radii. Interestingly, however, the derived $[Z/H]$ values (which are a combination of $[Fe/H]$ and $[E/Fe]$) show good agreement at all points except for the two high $[Z/H]$ inner points of SDSS0734. It is therefore evident that these differences arise as the result of the differing model set used (Thomas, Maraston & Bender in the multi-index fitting analysis and PegaseHR models in the ULYSS full spectral fitting analysis). With regards age, for SDSS0734 agreement is very good. However, the age gradient for SDSS0758 shows the largest discrepancy in our comparison. While we find a flat age gradient from multi-index fitting, we obtain systematically lower ages from full-spectrum fitting which even show a negative trend around $\log(r/r_{\text{eff}}) \sim -0.7$. We note that in this galaxy the deviations in age and $[Fe/H]$ follow the age-metallicity degeneracy, i.e. higher $[Fe/H]$ is compensated for by younger age. It is our intention to continue to make these comparisons in future data analyses in the hope of identifying consistent systematic difference between the model sets.

4 DISCUSSION

Figs. 3 and 4 show the spatially resolved stellar population parameters resulting from our analysis. It can be seen from Figure 3 that there is good agreement between values on either side of each axis and between the major and minor axes of each galaxy. This evidences the robustness of the multi-index fitting technique that we employ. However, we note that there is a hint of ellipticity in the $[Z/H]$ and perhaps $[Fe/H]$ profiles of SDSS0758 such that they decline faster along the minor axis. SDSS0758 has a minor/major axis ra-

tio of ~ 0.8 , which would cause a displacement in log radius of points along the minor axis of -0.1 with respect to the major axis values, consistent with the small displacement evident in Fig. 3. We detect no such displacement in SDSS0734, despite it exhibiting a similar ellipticity to SDSS0758.

The aim of this work is to begin the process of comparing the star formation histories and/or merger histories of the BCGs of fossil systems to those of normal systems. As well as the comparison of the central ages and metallicities of such systems, another, and potentially more powerful, approach is the comparison of the gradients in these parameters. As a result there has been much recent interest in the use of metallicity gradients as a probe of the merger histories of galaxies. However, such comparisons are severely hampered by the number of free parameters that describe the star formation and merger histories of large early-type galaxies, such as the BCGs in our sample. Key amongst these parameters are whether the mergers that the central galaxies experiences are wet or dry (whether or not there is significant gas present during the merger).

In the case of dry mergers the metallicity gradient of the merger remnant depends on both the mass ratio of the merger event and on the pre-merger gradients of the galaxies involved (e.g. Di Matteo et al. 2009). Conceivably, age gradients could also be produced in the case of dry mergers if the two merging galaxies have differing pre-merger ages.

For wet mergers, the effects on age gradients are generally more clearly defined, since the gas present in the merging galaxies is known to be funneled towards the galactic centers during the merger (e.g. Rupke et al. 2010), where bursts of star formation then take place (e.g. Ellison et al. 2013). These central starbursts then induce positive age gra-

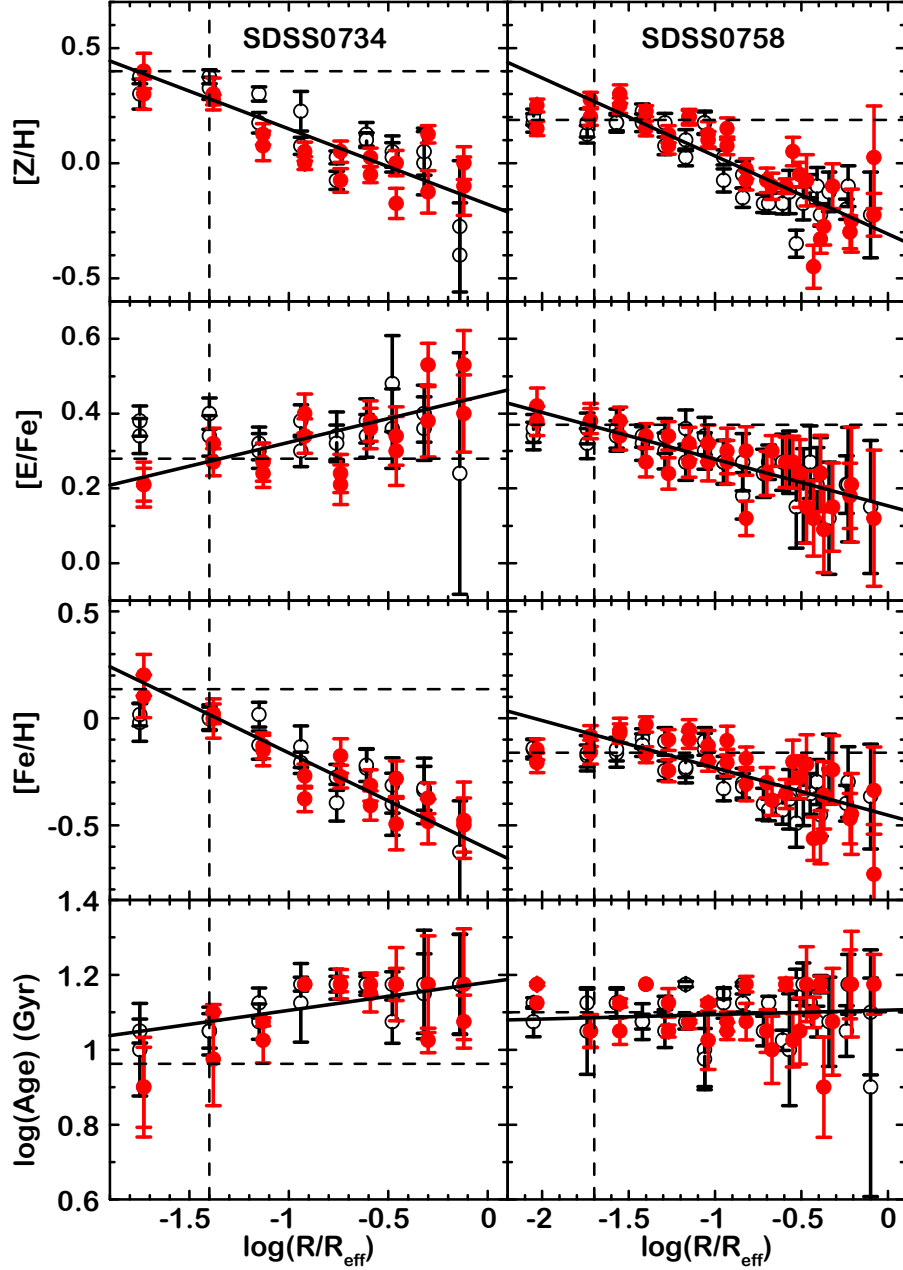


Figure 3. Spatially resolved stellar population parameters for the observed BCGs of fossil groups. The data are measured with the multi-index χ^2 -fitting technique detailed in Proctor & Sansom (2002). Filled, red points are measured along the major axis while open, black points present the minor axis. The horizontal dashed lines show the measured central values. The vertical lines indicate the typical seeing during our observations. Solid lines show linear least squares fits to the data.

dients (younger towards the centre). However, the prediction of metallicity gradients in merger remnants is *much* more complicated, since the gas driven to the centre of the merger remnant can drive the gradient either up or down depending on the specifics of the quantity, source and metallicity of the gas (Torrey et al. 2012).

Clearly, the interpretation of the gradients in individual galaxies is, at best, a complex process. This underlies the stated aim of this work - to begin the process of measuring gradients in fossil group BCGs in order to ultimately perform a *statistical* comparison to the BCGs of normal systems. In the following we

therefore refrain from attempting detailed interpretation of the individual galaxies, confining ourselves to general comments and comparisons between the individual galaxies.

Gradients of the stellar population parameters were obtained by fitting the radial profiles with linear relations of the form;

$$X[r/r_{\text{eff}}] = X_{\text{eff}} + \nabla_X \log(r/r_{\text{eff}}),$$

where X denotes the corresponding parameter. The fits have been weighted by the errors associated with each value. Gradients were computed excluding the seeing affected inner-

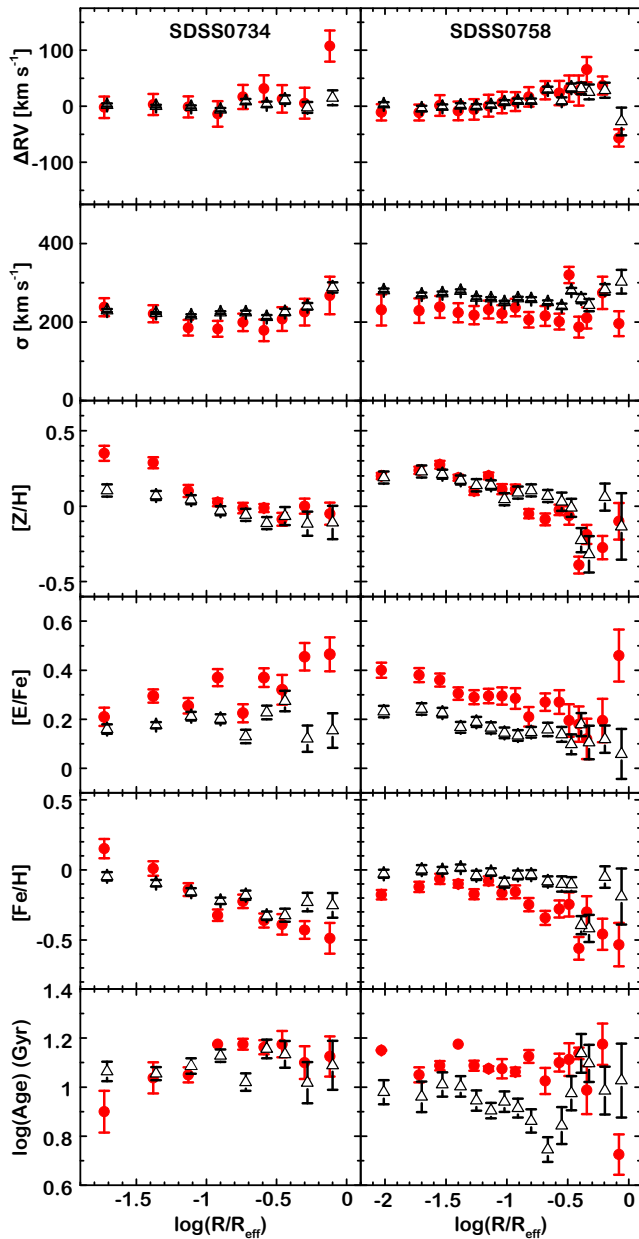


Figure 4. Comparison between the results from the multi-index χ^2 -fitting technique detailed in Proctor & Sansom (2002) and the full-spectrum fitting technique ULYSS. Red symbols show the major axis data from Fig.3, while open triangles show the results from full-spectrum fitting. In both cases the data have been folded along the major axis.

most point. We note that our derived gradients in general fit the data well out to the effective radius. The computed gradient slopes $\nabla_X \equiv \Delta X / \Delta \log(r/r_{\text{eff}})$ are given in Table 2. The significance of these gradients were tested using their correlation coefficients. All were found to be of greater than 3σ except for the $[E/Fe]$ in SDSS0758 (only 2σ) and $\log(\text{age})$ in SDSS0758 which in any case we find to exhibit no discernible gradient. The gradients in both galaxies were also found not to be significantly affected by the exclusion of the low signal-to-noise outer points.

We can readily see that despite the photometric similarities between the two galaxies, there are significant dif-

ferences in the radial gradients of their stellar population parameters.

Fig. 3 shows that, in SDSS0734 there is clear evidence that the central region of the galaxy is younger than its outer regions. There is also a suggestion that the central region has lower $[E/Fe]$ than the outer regions. Both $[Fe/H]$ and $[Z/H]$ show negative gradients over the whole radial range probed. This galaxy therefore appears to have formed either in a single burst, but star formation with the central regions continuing for 1-2 Gyr longer than in the out regions i.e. long enough for Type Ia supernovae to begin driving the central $[E/Fe]$ down, or the galaxy may have formed an old population upon which a central burst was then superimposed a few Gyr later. In either case we might characterise the central regions of this galaxy as having formed over a relatively extended period of time.

In SDSS0758, on the other hand, the galaxy exhibits no detectable age gradient but a negative $[E/Fe]$ gradient. Although the galaxy also exhibits negative $[Fe/H]$ and $[Z/H]$ gradients, there is a strong suggestion of a flattening in this gradient in the central regions. Indeed the $[Fe/H]$ gradient appears to be flat all the way out to $\log(r/r_{\text{eff}}) = -1$, and from our full-spectrum fitting results, we measure a flat gradient even out to $\log(r/r_{\text{eff}}) = -0.5$. The $[E/Fe]$ gradient in this galaxy suggests that this galaxy also formed over a relatively extended period of time, except in this case the later star formation took place in the outer regions, rather than in the central regions as was the case in SDSS0734. This galaxy therefore resembles a bulge and disc galaxy in which star formation was truncated very early, but slightly later (perhaps ~ 1 Gyr) in the outer regions. This is supported by the flat (perhaps even negative) $[Fe/H]$ gradient in the central region which can arise if star formation in the central was truncated prior to the star formation further out.

It is the aim of this project to compare the BCGs of fossil galaxy groups with BCGs in non-fossil aggregates. However, with a sample of only two galaxies we can draw no firm conclusions at this point, other than to note that these galaxies possess stellar population parameters and gradients consistent with the range of values exhibited by normal BCGs (Loubser & Sánchez-Blázquez 2012).

5 CONCLUSIONS

We have presented spatially resolved stellar population parameters $\log(\text{age})$, $[Fe/H]$, $[Z/H]$ and $[E/Fe]$ for two first-ranked fossil group galaxies, SDSS0734 and SDSS0758. These two galaxies have quite different stellar population parameters, despite their similarities in morphology, absolute magnitude, colour and central velocity dispersions, as well as the groups in which they reside. We suggest that one of them, SDSS0734, may have had a recent central burst of star formation superimposed onto an old stellar population, which explains a positive age gradient, a steep negative metallicity gradient and positive $[E/Fe]$ gradient. For the other galaxy, SDSS0758, however, a well-known X-ray AGN (Sun 2009), we argue that the star formation was complete ~ 10 Gyr ago. However, the negative gradient in $[E/Fe]$ and flat central metallicity profile suggest that star formation may have continued slightly longer in the outer regions than in the central regions of the galaxy (i.e. inside out formation).

Table 2. Central values and radial gradients of the measured stellar population parameters. System velocities and central velocity dispersions are also given. Errors are listed below the corresponding values.

	RV	σ_0	$\log(\text{age})_0$	$[\text{Fe}/\text{H}]_0$	$[\text{E}/\text{Fe}]_0$	$[\text{Z}/\text{H}]_0$	$\nabla \log(\text{age})$	$\nabla [\text{Fe}/\text{H}]$	$\nabla [\text{E}/\text{Fe}]$	$\nabla [\text{Z}/\text{H}]$
SDSS0734	23868	254	0.96	0.14	0.28	0.40	0.08	-0.45	0.13	-0.33
	6	17	0.01	0.01	0.04	0.03	0.05	0.07	0.07	0.10
SDSS0758	12209	224	1.10	-0.16	0.37	0.19	0.01	-0.22	-0.13	-0.34
	9	9	0.03	0.02	0.03	0.01	0.06	0.09	0.05	0.09

Our results therefore suggest that there may be considerable dispersion in the range of measured stellar population parameters of first-ranked galaxies in fossil groups. We plan to study a larger sample of these galaxies in detail in order to have a better notion of how the central galaxies in fossil groups formed and to investigate if there are any differences in their properties with respect to the properties of non-fossil BCGs.

ACKNOWLEDGMENTS

This work is based on observations obtained at the Gemini Observatory, which is operated by the Association of Universities for Research in Astronomy, Inc., under a cooperative agreement with the NSF on behalf of the Gemini partnership: the National Science Foundation (United States), the Science and Technology Facilities Council (United Kingdom), the National Research Council (Canada), CONICYT (Chile), the Australian Research Council (Australia), Ministério da Ciência e Tecnologia (Brazil) and Ministerio de Ciencia, Tecnología e Innovación Productiva (Argentina). This research made use of NASA's Astrophysics Data System, as well as IRAF and STARLINK software. IRAF is distributed by the National Optical Astronomy Observatories, which is operated by the Association of Universities for Research in Astronomy, Inc. (AURA) under cooperative agreement with the National Science Foundation. RNP acknowledges financial support from the Brazilian agency FAPESP (program number 2008/57331-0). CMdO also acknowledges FAPESP (program number 2006/56213-9) and CNPq. PE acknowledges support from FONDECYT through grant 3130485. We thank Mina Koleva for useful discussions on the full-spectrum fitting package ULYSS.

REFERENCES

- Adelman-McCarthy J.K. et al. 2008, ApJS, 175, 297
 Brough S., Proctor R., Forbes D.A., Couch W.J., Burke D.J., Mann R.G., 2007, MNRAS, 378, 1507
 Bruzual G., Charlot S., 2003, MNRAS, 344, 1000
 Carter D., Bridges T.J., Hau G.K.T., 1999, MNRAS, 307, 131
 D'Onghia E., Sommer-Larsen J., Romeo A.D., Burkert A., Pedersen K., Portinari L., Rasmussen J., 2005, ApJ, 630, 109
 Díaz-Giménez E., Muriel H., Mendes de Oliveira C., 2008, A&A, 490, 965
 Dariush A., Khosroshahi H.G., Ponman T.J., Pearce F., Raychaudhury S., Hartley W., 2007, MNRAS, 382, 433
 Davidge T.J., Grindler M., 1995, AJ, 109, 1433
 Di Matteo P., Pipino A., Lehnert M.D., Combes F., Semelin B., 2009, A&A, 499, 427

- Eigenthaler P., Zeilinger W.W., 2013, A&A, 553, 99
 Ellison S.L., Mendel J.T., Patton D.R., Scudder J.M., accepted MNRAS
 Fisher D., Franx M., Illingworth G., 1995, ApJ, 448, 119
 Gorgas J., Efstathiou G., Aragon-Salamanca A., 1990, MNRAS, 245, 217
 Jones L.R., Ponman T.J., Horton A., Babul A., Ebeling H., Burke D.J., 2003, MNRAS, 343, 627
 Koleva M., Prugniel P., Bouchard A., Wu Y., 2009, A&A, 501, 1269
 Le Borgne D., Rocca-Volmerange B., Prugniel P., Lançon A., Fioc M., Soubiran C., 2004, A&A, 425, 881
 Loubser S.I., Sánchez-Blázquez P., 2012, MNRAS, 425, 841
 Loubser S.I., Sánchez-Blázquez P., Sansom A.E., Soechting I.K., 2009, MNRAS, 398, 133
 Mehlert D., Thomas D., Saglia R.P., Bender R., Wegner G., 2003, A&A, 407, 423
 Proctor R.N., Sansom, A.E., 2002, MNRAS, 333, 517
 Proctor R.N., Lah P., Forbes D.A., Colless M., Couch W., 2008, MNRAS, 386, 1781
 Prugniel P., Soubiran C., 2001, A&A, 369, 1048
 Prugniel P., Koleva, M. 2012, IAUS, 284, 16
 Rupke D.S.N., Kewley L.J., Chien L.-H., 2010, ApJ, 723, 1255
 Sánchez-Blázquez P., Gorgas J., Cardiel N. 2006, A&A, 457, 823
 Skrutskie, M. F. et al. 2006, AJ, 131, 1163
 Spolaor M., Proctor R.N., Forbes D.A., Couch W.J., 2009, ApJ, 691, 138
 Sun, M. 2009, ApJ, 704, 1586
 Torrey P., Cox T.J., Kewley L., Hernquist L., 2012 ApJ, 746, 108
 von der Linden A., Best P.N., Kauffmann G., White S.D.M., 2007, MNRAS, 379, 867
 Worthey G., Faber S.M., Gonzalez J.J., Burstein D., 1994, ApJS, 94, 687
 Worthey, G., Ottaviani, D. L. 1997, ApJS, 111, 377
 Wu, Y. et al. 2011, A&A, 525, 71

APPENDIX A: KINEMATIC PROPERTIES

APPENDIX B: STELLAR POPULATION PARAMETERS

Table A1. Kinematic data for SDSS0734. Results are shown for both major and minor axes.

$\log(r/r_{\text{eff}})$	major axis		minor axis	
	ΔRV	σ	ΔRV	σ
0.07	-47(27)	178(42)	134(41)	175(70)
-0.12	116(32)	270(52)	82(77)	150(76)
-0.30	-3(25)	194(34)	41(25)	224(50)
-0.46	10(27)	161(33)	0(26)	242(47)
-0.59	41(27)	194(40)	18(25)	228(40)
-0.74	27(27)	187(33)	44(25)	182(35)
-0.92	-15(29)	182(29)	21(28)	232(36)
-1.13	1(28)	186(30)	16(29)	190(32)
-1.38	5(27)	230(33)	16(27)	193(31)
-1.73	-13(28)	265(36)	25(27)	208(32)
Centre	12(25)	237(34)	-11(25)	270(32)
-1.73	-10(26)	211(28)	1(26)	209(37)
-1.38	-2(26)	212(28)	-2(28)	210(31)
-1.13	4(25)	185(27)	-6(33)	195(31)
-0.92	12(35)	184(28)	-7(29)	180(29)
-0.74	-7(33)	211(30)	-13(41)	187(30)
-0.59	-22(39)	164(38)	-12(49)	204(30)
-0.46	-16(41)	254(51)	-12(46)	139(31)
-0.30	-14(49)	256(59)	-13(49)	83(35)
-0.12	-99(45)	265(81)	93(47)	150(45)
0.06	-68(46)	198(46)	5(48)	150(48)

Table A2. Kinematic data for SDSS0758. Results are shown for both major and minor axes.

$\log(r/r_{\text{eff}})$	major axis		minor axis	
	ΔRV	σ	ΔRV	σ
-0.08	-172(22)	196(44)	-81(31)	78(57)
-0.22	15(20)	353(72)	32(33)	156(43)
-0.37	14(21)	294(39)	10(22)	170(30)
-0.43	9(20)	171(38)	11(20)	213(31)
-0.51	5(19)	260(25)	28(19)	250(30)
-0.59	-3(19)	221(29)	12(19)	221(20)
-0.70	3(22)	221(40)	-14(22)	161(18)
-0.82	-2(26)	206(25)	18(33)	198(38)
-0.93	0(27)	227(29)	10(34)	189(26)
-1.04	-17(32)	236(32)	-14(35)	206(18)
-1.15	-24(33)	234(30)	5(33)	197(28)
-1.27	-36(30)	216(28)	-10(30)	190(26)
-1.40	-38(26)	198(30)	-18(26)	211(27)
-1.55	-30(27)	231(37)	51(27)	202(36)
-1.72	-37(21)	249(40)	35(21)	223(38)
-2.03	-22(21)	248(52)	28(21)	217(35)
Centre	-19(19)	215(55)	29(19)	232(33)
-2.03	-1(20)	214(59)	-15(20)	216(35)
-1.72	-15(19)	209(48)	-15(19)	218(30)
-1.55	-33(25)	246(42)	-13(25)	200(23)
-1.40	-21(21)	249(39)	3(30)	185(27)
-1.27	-24(20)	220(37)	-35(37)	207(18)
-1.15	-26(21)	230(34)	-58(38)	199(17)
-1.04	-30(21)	206(29)	-61(41)	239(17)
-0.93	-17(20)	247(34)	-50(49)	196(19)
-0.82	-36(23)	206(30)	-54(41)	197(18)
-0.67	-54(24)	210(31)	-42(46)	174(28)
-0.55	-50(39)	181(29)	-87(39)	241(29)
-0.47	-58(43)	380(33)	-60(43)	276(31)
-0.39	-47(50)	204(37)	-75(50)	197(26)
-0.32	-117(40)	127(37)	21(40)	184(40)
-0.21	-59(25)	196(40)	-37(52)	251(47)
-0.08	-59(22)	196(45)	-99(54)	172(58)

Table B1. Measured stellar population parameters for SDSS0734. Results are shown for both major and minor axes. Errors are given in brackets. Log(age) is expressed in Gyr.

major axis					minor axis			
$\log(r/r_{\text{eff}})$	$\log(\text{age})$	[Fe/H]	[E/Fe]	[Z/H]	$\log(\text{age})$	[Fe/H]	[E/Fe]	[Z/H]
-0.12	1.175(0.148)	-0.50(0.18)	0.53(0.10)	0.00(0.13)	1.175(0.134)	-1.03(0.24)	0.80(0.32)	-0.28(0.23)
-0.30	1.025(0.033)	-0.37(0.07)	0.53(0.06)	0.13(0.04)	1.150(0.106)	-0.34(0.15)	0.36(0.09)	0.00(0.14)
-0.46	1.175(0.043)	-0.28(0.08)	0.30(0.09)	0.00(0.06)	1.075(0.058)	-0.40(0.15)	0.48(0.13)	0.05(0.07)
-0.59	1.175(0.030)	-0.41(0.07)	0.38(0.05)	-0.05(0.04)	1.175(0.029)	-0.23(0.09)	0.38(0.06)	0.13(0.05)
-0.74	1.175(0.039)	-0.27(0.05)	0.21(0.05)	-0.08(0.05)	1.175(0.040)	-0.40(0.09)	0.34(0.06)	-0.08(0.04)
-0.92	1.175(0.000)	-0.38(0.06)	0.40(0.05)	0.00(0.03)	1.125(0.105)	-0.13(0.10)	0.38(0.04)	0.23(0.09)
-1.13	1.025(0.060)	-0.15(0.07)	0.24(0.04)	0.08(0.07)	1.125(0.040)	-0.13(0.07)	0.32(0.04)	0.18(0.04)
-1.38	0.975(0.125)	0.00(0.09)	0.32(0.04)	0.30(0.07)	1.050(0.064)	0.01(0.06)	0.34(0.05)	0.33(0.05)
-1.73	0.900(0.133)	0.20(0.10)	0.21(0.04)	0.40(0.08)	1.000(0.124)	-0.02(0.09)	0.34(0.05)	0.30(0.07)
Centre	0.975(0.158)	0.15(0.06)	0.24(0.04)	0.38(0.06)	0.950(0.103)	0.12(0.06)	0.32(0.04)	0.43(0.05)
-1.73	0.900(0.107)	0.10(0.10)	0.21(0.06)	0.30(0.07)	1.050(0.032)	0.02(0.05)	0.38(0.04)	0.38(0.03)
-1.38	1.100(0.021)	0.02(0.05)	0.27(0.04)	0.28(0.02)	1.050(0.046)	0.00(0.06)	0.40(0.04)	0.38(0.03)
-1.13	1.075(0.011)	-0.13(0.06)	0.27(0.05)	0.13(0.05)	1.075(0.047)	0.02(0.06)	0.30(0.05)	0.30(0.03)
-0.92	1.175(0.000)	-0.27(0.06)	0.34(0.05)	0.05(0.04)	1.175(0.019)	-0.21(0.05)	0.30(0.04)	0.08(0.04)
-0.74	1.175(0.020)	-0.18(0.08)	0.24(0.05)	0.05(0.05)	1.175(0.021)	-0.28(0.06)	0.32(0.05)	0.03(0.02)
-0.59	1.150(0.049)	-0.31(0.07)	0.36(0.05)	0.03(0.04)	1.175(0.021)	-0.22(0.08)	0.34(0.06)	0.10(0.03)
-0.46	1.175(0.098)	-0.50(0.12)	0.34(0.08)	-0.18(0.07)	1.175(0.033)	-0.31(0.13)	0.36(0.11)	0.03(0.06)
-0.30	1.175(0.129)	-0.48(0.10)	0.38(0.10)	-0.13(0.09)	1.175(0.145)	-0.33(0.10)	0.40(0.08)	0.05(0.10)
-0.12	1.075(0.071)	-0.50(0.13)	0.53(0.09)	0.00(0.07)	1.175(0.133)	-1.03(0.21)	0.80(0.28)	-0.28(0.29)

Table B2. Measured stellar population parameters for SDSS0758. Results are shown for both major and minor axes. Errors are given in brackets. Log(age) is expressed in Gyr.

major axis					minor axis			
$\log(r/r_{\text{eff}})$	$\log(\text{age})$	[Fe/H]	[E/Fe]	[Z/H]	$\log(\text{age})$	[Fe/H]	[E/Fe]	[Z/H]
-0.08	1.175(0.080)	-0.34(0.20)	0.12(0.18)	-0.23(0.09)	1.100(0.167)	-1.43(0.19)	0.80(0.12)	-0.68(0.16)
-0.22	1.175(0.092)	-0.47(0.12)	0.18(0.08)	-0.30(0.07)	1.050(0.068)	-0.40(0.08)	0.21(0.08)	-0.20(0.04)
-0.37	0.900(0.134)	-0.36(0.16)	0.09(0.12)	-0.28(0.08)	1.175(0.023)	-0.45(0.10)	0.24(0.10)	-0.23(0.05)
-0.43	1.100(0.041)	-0.56(0.10)	0.12(0.10)	-0.45(0.09)	1.125(0.034)	-0.35(0.10)	0.27(0.10)	-0.10(0.05)
-0.51	1.050(0.088)	-0.28(0.10)	0.24(0.09)	-0.05(0.05)	1.175(0.040)	-0.49(0.11)	0.15(0.11)	-0.35(0.06)
-0.59	1.175(0.016)	-0.35(0.07)	0.27(0.07)	-0.10(0.03)	1.025(0.027)	-0.43(0.07)	0.27(0.08)	-0.18(0.05)
-0.70	1.050(0.057)	-0.30(0.07)	0.24(0.06)	-0.08(0.05)	1.050(0.040)	-0.40(0.07)	0.24(0.06)	-0.18(0.04)
-0.82	1.175(0.021)	-0.19(0.05)	0.12(0.05)	-0.08(0.04)	1.175(0.005)	-0.30(0.07)	0.27(0.08)	-0.05(0.06)
-0.93	1.050(0.023)	-0.21(0.06)	0.30(0.06)	0.08(0.04)	1.125(0.041)	-0.33(0.06)	0.27(0.06)	-0.08(0.05)
-1.04	1.125(0.008)	-0.20(0.05)	0.32(0.05)	0.10(0.04)	1.000(0.099)	-0.15(0.08)	0.34(0.05)	0.18(0.05)
-1.15	1.075(0.019)	-0.05(0.05)	0.27(0.04)	0.20(0.03)	1.075(0.020)	-0.24(0.06)	0.36(0.05)	0.10(0.05)
-1.27	1.050(0.016)	-0.10(0.05)	0.24(0.04)	0.13(0.04)	1.125(0.018)	-0.25(0.05)	0.34(0.05)	0.08(0.04)
-1.40	1.175(0.000)	-0.17(0.04)	0.34(0.03)	0.15(0.03)	1.075(0.020)	-0.10(0.05)	0.34(0.03)	0.23(0.03)
-1.55	1.125(0.011)	-0.07(0.04)	0.34(0.04)	0.25(0.03)	1.125(0.041)	-0.16(0.07)	0.36(0.05)	0.18(0.04)
-1.72	1.050(0.043)	-0.08(0.05)	0.38(0.03)	0.28(0.03)	1.125(0.037)	-0.18(0.05)	0.32(0.04)	0.13(0.04)
-2.03	1.125(0.000)	-0.15(0.05)	0.42(0.05)	0.25(0.03)	1.075(0.040)	-0.15(0.05)	0.34(0.04)	0.18(0.04)
Centre	1.125(0.004)	-0.18(0.05)	0.40(0.04)	0.20(0.03)	1.075(0.039)	-0.15(0.05)	0.34(0.03)	0.18(0.04)
-2.03	1.175(0.004)	-0.21(0.04)	0.38(0.04)	0.15(0.03)	1.125(0.014)	-0.14(0.04)	0.36(0.04)	0.20(0.04)
-1.72	1.050(0.044)	-0.16(0.06)	0.38(0.05)	0.20(0.04)	1.050(0.116)	-0.16(0.08)	0.36(0.04)	0.18(0.06)
-1.55	1.050(0.036)	-0.06(0.06)	0.38(0.04)	0.30(0.04)	1.125(0.037)	-0.15(0.06)	0.34(0.04)	0.18(0.03)
-1.40	1.175(0.000)	-0.03(0.04)	0.27(0.04)	0.23(0.02)	1.075(0.048)	-0.13(0.05)	0.32(0.05)	0.18(0.04)
-1.27	1.125(0.038)	-0.25(0.05)	0.34(0.04)	0.08(0.04)	1.050(0.044)	-0.11(0.06)	0.30(0.05)	0.18(0.04)
-1.15	1.075(0.004)	-0.10(0.04)	0.32(0.04)	0.20(0.03)	1.175(0.007)	-0.23(0.05)	0.27(0.05)	0.03(0.04)
-1.04	1.025(0.078)	-0.13(0.07)	0.27(0.05)	0.13(0.06)	0.975(0.082)	-0.11(0.06)	0.30(0.05)	0.18(0.05)
-0.93	1.075(0.026)	-0.10(0.07)	0.27(0.06)	0.15(0.05)	1.150(0.014)	-0.23(0.05)	0.27(0.06)	0.03(0.03)
-0.82	1.075(0.049)	-0.31(0.08)	0.30(0.07)	-0.03(0.04)	1.125(0.024)	-0.32(0.06)	0.18(0.06)	-0.15(0.04)
-0.67	1.000(0.090)	-0.38(0.07)	0.30(0.04)	-0.10(0.06)	1.125(0.018)	-0.43(0.05)	0.27(0.05)	-0.18(0.04)
-0.55	1.025(0.071)	-0.20(0.10)	0.27(0.07)	0.05(0.06)	1.000(0.150)	-0.38(0.14)	0.27(0.08)	-0.13(0.09)
-0.47	1.175(0.100)	-0.22(0.14)	0.15(0.10)	-0.08(0.11)	1.175(0.057)	-0.35(0.16)	0.18(0.13)	-0.18(0.07)
-0.39	1.175(0.021)	-0.56(0.16)	0.24(0.10)	-0.33(0.06)	1.075(0.041)	-0.30(0.10)	0.21(0.10)	-0.10(0.08)
-0.32	1.075(0.143)	-0.24(0.16)	0.15(0.12)	-0.10(0.10)	1.075(0.119)	-0.24(0.16)	0.12(0.15)	-0.13(0.09)
-0.21	1.175(0.141)	-0.45(0.19)	0.21(0.15)	-0.25(0.14)	1.175(0.080)	-0.30(0.17)	0.21(0.15)	-0.10(0.09)
-0.08	0.275(0.143)	-0.73(0.24)	0.80(0.11)	0.03(0.22)	0.900(0.292)	-0.37(0.24)	0.15(0.18)	-0.23(0.19)